Lab on a Chip

This is an *Accepted Manuscript*, which has been through the Royal Society of Chemistry peer review process and has been accepted for publication.

Accepted Manuscripts are published online shortly after acceptance, before technical editing, formatting and proof reading. Using this free service, authors can make their results available to the community, in citable form, before we publish the edited article. We will replace this *Accepted Manuscript* with the edited and formatted *Advance Article* as soon as it is available.

You can find more information about *Accepted Manuscripts* in the **Information for Authors**.

Please note that technical editing may introduce minor changes to the text and/or graphics, which may alter content. The journal's standard **Terms & Conditions** and the **Ethical guidelines** still apply. In no event shall the Royal Society of Chemistry be held responsible for any errors or omissions in this *Accepted Manuscript* or any consequences arising from the use of any information it contains.

Cross polarization compatible dialysis chip

Micha Kornreich,^{a¶} Michael Heymann,^{bc¶‡}, Seth Fraden^{c*} and Roy Beck^{a*}

We visualize birefringence in μL sample volumes using a microfluidic dialysis chip optimized for cross polarization microscopy. The chip is composed of two overlapping Polydimethylsiloxane (PDMS) channels separated by a commercial cellulose ester membrane. Buffer exchange in the sample chamber is achieved within minutes by dialyzing under continuous reservoir flow. Using fd virus as a birefringent model system we monitor the fd virus isotropic to liquid crystal phase transition as a function of ionic strength. We show that the reorientation of the fd virus spans a few 10s of seconds, indicative of a fast ion exchange across the membrane. Complete phase separation re-organization takes minutes to hours as it involves diffusive virus mass transport within the storage chamber.

Introduction

Birefringence measurements are widely applied in medical diagnostics and bio-material research, as it is a non-destructive, non-intrusive method that can provide long range structural information. For example in ex-vivo tissue examinations it is used to monitor myocardial regeneration[1] and to assess thermal injury in cardiac muscle[2]. Congo Red stained amyloid fibrils and plaques, like those associated with Alzheimer's disease, are birefringent[3]. Medical diagnostic uses also include a definitive diagnosis of gout, through identification of monosodium urate crystals in synovial fluid under polarized light microscopy[4]; sperm heads characterization or the selection of reacted spermatozoa for intra-cytoplasmic sperm injection[5]; and optically measuring nerve thickness for the early detection of glaucoma[6].

Cross polarizing microscopy is widely used to characterize crystals and liquid crystals in crystallization assays[7] and when mapping phase diagrams of organic and biological samples[8–10] or for example to monitor the assembly of DNA origami phases[11]. In such experiments, several variables like temperature, pH, sample concentrations, ionic strength and other neutral osmolytes are usually probed. To accurately determine phase boundaries, repeated sampling is necessary. Yet, biological samples such as tissue preparations or purified proteins are often precious.

A microfluidic dialysis method, which is compatible with cross polarizing microscopy, could overcome these constraints of the small sample quantities available and the need for repeated sampling. Microfluidic devices with filtration membranes of different pore size provide reversible control over buffer composition, by exchanging desired solutes based on their molecular weight. The incorporation of custom and commercial membranes is common and several alternatives are available[12–14]. Such membrane chips have already been used to study phase transitions[10]. Also, many spectroscopic and microscopic methods were successfully integrated with microfluidic devices in general, including optical tweezers[15], fluorescence microscopy[16], raman spectroscopy[17], dynamic and static light scattering[18,19], various optical sensors[20] and X-ray diffraction and imaging[21]. However, the combination of dialysis with cross polarisation microscopy is challenging, because dialysis membranes are usually highly birefringent themselves. Even when the membrane source material is not polarising, the final membrane can become polarising when stress induced birefringence is 'frozen' in during manufacturing or due to anisotropic elasticity of the membrane.

In this paper we describe and validate a cross polarizing compatible microfluidic dialysis device, using the filamentous bacteriophage fd as a model system. Our device allows to combine birefringent-based analysis and diagnostic methods with the microfluidic advantages of small sample consumption and fast assay rates, which we found to be on the order of minutes. By choosing the appropriate molecular weight cutoff, it is easy to exchange buffer without diluting the stored sample. This allows the efficient study of phase transitions, like crystallization and gelation. Multiple buffer conditions may be tested on a single sample by repeatedly exchanging the reservoir buffer without loading a new sample, if the transition is reversible as was the case with our fd virus model

^{a} *The Raymond and Beverly Sackler School of Physics and Astronomy, Tel-Aviv University, 69978 Tel Aviv, Israel. E-mail: roy@post.tau.ac.il*
^{b} *Biophysics and Structural Biology Program, Graduate School of Arts and Sciences, Brandeis University, Waltham, Massachusetts, USA*
^{c} *Department of Physics, Graduate School of Arts and Sciences, Brandeis University, Waltham, Massachusetts, USA*
¶ *These authors contributed equally to this work.*
‡ Present address: Center for Free Electron Laser Science, Hamburg, Germany

system. Samples that aggregate upon buffer exchange, such as amyloids, may be pre-loaded in their soluble form to then dialyze the assembly buffer into the sample chamber.

Dialysis chip design, fabrication and validation

Choice of materials: To build a microfluidic dialysis chamber compatible with polarization microscopy, all its components must be transparent and at the most have a birefringence smaller then the sample investigated. While glass and PDMS are transparent and not birefringent, most commercial dialysis membranes are either opaque or highly birefringent. From all tested membranes, we found cellulose ester (CE) membranes to be transparent and to have a low birefringence, as measured by a Berek compensator on an Olympus BX51 polarisation microscope (ESI table). Commercial CE membranes are also comparably thin (60 μm), which minimizes diffusion times between sample and reservoir channels; an important feature for time resolved experiments. Another advantage of the CE membrane is the wide range of available pore sizes. Pore sizes spanning from nanofiltration to microfiltration cutoffs, as well as low protein binding CE membranes allow for versatile uses in material and biological sciences.

Chip fabrication: We assembled a device from separate, detachable components, such that the membrane is contained between the two microfluidic chip halves, one for sample storage and the other one for reservoir perfusion[22] (Fig. 1). Thin 350 μm PDMS slabs (Sylgard 184, Dow Corning) containing the features were fabricated using standard soft-lithography[23] and mounted between 1 mm thick glass slides that were clamped together using acrylic plates and screws. The membrane was mechanically compressed between the two PDMS halves, which covered the entire membrane surface. The glass support allowed for a minimum working distance of 1.4 mm. The PDMS reservoir layer had 200 μm wide channels shaped into a serpentine spaced 350 μm apart to facilitate fast buffer exchange by maximising the accessible membrane, while also offering mechanical support to minimize channel collapse and bending (Fig. 1b). The second PDMS layer for sample storage was separated from the first one by the 60 μm thick CE membrane. Two sample storage channels were 200 μm deep, 1000 μm wide and 5000 μm long. The total volume for each storage channel was thus 1 μL. The PDMS slabs and supporting microscope glass slides were held in place and gently clamped together using acrylic plates (McMaster Carr) cut to shape with a 40 W CO_2 laser cutter (Hobby Laser, Full Spectrum Laser) and fastened manually using screws. Since the acrylic plastic is birefringent, windows of 2 by 2 cm were cut out on the top and bottom plates for polarized light to go through unperturbed.

The device is modular and can therefore be disassembled, cleaned and reused multiple times. The chip was leak free for
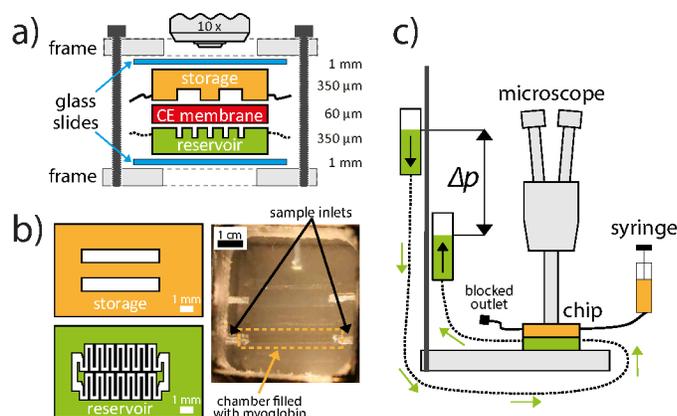

Fig. 1 Chip assembly and operation. (a) Side view and (b, left) top view schematic of the chip and PDMS channels. (b, right) Photograph of the chip as seen through the top window. For illustration, one storage channel was stained red using a myoglobin solution. (c) Reservoir inlet and outlet were connected to vials that were open to atmospheric pressure and mounted on a vertical rail. This allowed to control reservoir flow and pressure by changing the height (Δp) difference between reservoir inlet and outlet vials.

many days, as verified by a concentrated myoglobin (Sigma-Aldrich) solution (Fig. 1b). When assembled with a membrane larger than the PDMS slabs, the protruding membrane ends were wetted, but no protein diffusion was observed.

Sample loading: The chip was loaded using and injection loop and fluorophilic oil to minimize sample consumption, as detailed in the supporting information (Fig ESI1). The chip was placed on a rotating stage of a Olympus BX51 cross polarized microscope. Time lapse images were taken by an AVT Marlin firewire color camera (Allied Vision Technologies) for the duration of each experiment.

On-chip dialysis: Hydrostatic pressure driven flow was used to control on-chip dialysis (Fig. 1c). It was chosen to prevent pressure building up inside the chip uncontrollably, as can be the case when operating microfluidic devices under constant flow with syringe pumps. This is important, because water can be pushed through the dialysis membrane against a concentration gradient in a process known as reverse osmosis. For example, in initial experiments performed under constant flow, a storage channel initially filled with oil only, nucleated aqueous "puddles" growing on the membrane. This was most likely due to water being pushed from the reservoir across the membrane into the storage layer. To prevent such "leakage" from the reservoir into the storage layer, we performed control experiments to determine the vial positions corresponding to the maximal pressure differences, at which no droplets were observed over a period of 3 days.

***fd* Virus Experiment:** To test on chip dialysis we chose *fd* virus, a filamentous bacteriophage that forms cholesteric

liquid crystals[24]. A single fd virus can be described as a rod-like semiflexible charged polymer of length 0.88 μm, hard rod diameter 6.6 nm, persistence length 2.2 mm and linear charge density of 10 e^-/nm at pH 8.15[25]. These properties, in addition to its structural homogeneity, makes it an ideal model system for studying liquid crystal phase transitions in biopolymers.

Suspensions of fd virus undergo an isotropic to nematic phase transition[26] by simply increasing the ionic strength of the surrounding buffer at constant virus concentration. This phase transition was explained by Onsager as occurring at a volume fraction $\phi_{IN} = 4\frac{D_{eff}}{L}$, or equivalently, number density $n_{IN} = \frac{16}{\pi L^2 D_{eff}}$. Onsager showed that the virus can be considered to have a salt dependent hard-rod equivalent diameter, D_{eff}, which is large at low ionic strength and shrinks towards the hard rod diameter as ionic strength is increased. If the fd virus number concentration $n > n_{IN}$ then the sample is nematic, but by raising ionic strength D_{eff} is lowered and therefore n_{IN} is increased. If the ionic strength is raised enough such that the condition $n < n_{IN}$ is achieved, the virus solution will turn isotropic.

We grew and purified fd virus as described previously[27]. A stock solution with 40 mg/ml fd virus in 20 mM Tris-HCl, pH 8.15 and a dextran volume fraction of $\phi_{dextran} = 0.6$ using dextran with 148 kDa molecular weight was prepared. The volume fraction was calculated by $\phi_{dextran} = \rho \frac{4}{3}\pi R_g^3$, where ρ is the polymer number density and R_g the radius of gyration of dextran. The radius of gyration was approximated as R_g [Å] $= 0.66(M)^{0.43} = 110$ Å, where M is in units of gr/mol[28]. fd virus concentrations were determined by U.V. absorption measurements[29], using an extinction coefficient of A(269nm) $= 3.84$ for a path length of 1 cm and 1 mg/ml. All reservoir solutions used contained 20 mM Tris-HCl, pH 8.15, $\phi_{dextran} = 0.6$ and varying concentrations of NaCl. In all experiments we used a CE membrane with 50 kDa molecular weight cut off to prevent fd virus and dextran leakage across the membrane, while allowing for fast exchange of ions.

To probe the fd virus phase dependence on ionic strength, we varied NaCl concentrations, while keeping a constant concentration of 40 mg/ml fd virus in the storage layer. At the initial condition of 0 mM NaCl, the fd virus suspension was in the nematic phase, which was strongly birefringent and easily visible using polarization microscopy (Fig. 2a). Tris buffers with increasing salt concentrations were washed into the reservoir from the overhanging vial, while time lapse images were recorded with the cross polarizing microscope. For each such buffer exchange we allowed for full liquid crystal phase equilibration before introducing a new salt condition to probe the next point in the phase diagram.

A transition from a single nematic phase to two distinct nematic and isotropic phases was observed at 120 mM NaCl, in agreement with previous bulk results[24]. The transition occurred gradually over an hour, with smooth cholesteric lines slowly being being broken into granular-looking smaller nematic elliptic domains (Fig. 2f, inset). This transition was reversible and the single nematic state was restored upon reducing the present salt concentration to below 100 mM NaCl and waiting a few hours for complete re-equilibration.

While the equilibrium phases were reproducible regardless of previous NaCl concentrations, the phase transition kinetics and domain sizes depended strongly on sample history. Nevertheless, transition kinetics could be divided into two distinct categories: fast, of duration of several minutes, and slow, hour-long transitions. When changing salt between any two concentrations within the range of 0 to 100 mM NaCl, the virus liquid crystal re-equilibrated within minutes of the buffer change (Fig. 2a-d). Transitions involving salt concentrations exceeding 120 mM NaCl required a few hours to re-equilibrate (Fig. 2e-f). For example, increasing salt from 0 to 280 mM NaCl resulted initially in a rapid deformation of nematic domains which caused a substantial decrease in the crossed polarized light intensity (Fig. ESI2), followed by a slow, hours long transition to isotropic-nematic co-existence. The latter slow dynamic phase transition gave rise to re-illuminated crossed polarized light intensity. Furthermore, this co-existence regime was composed of circa 30 μm long nematic tactoids of elliptic shape that where surrounded by large areas of isotropic order (Fig. 2f). Similarly, equilibration took several hours after the salt concentration had been lowered from 280 mM to below 120 mM NaCl to drive the transition from the two phase isotropic-nematic coexistence back to the single nematic phase. However, in this case no rapid initial response were observed.

It should be noted that the observed hour-long transition cannot be attributed to ion diffusion. The diffusion coefficient of NaCl is approximately $\sim 1.5 \cdot 10^3$ μm^2/s for 0 to 280 mM NaCl concentration in water[30], and is unaffected by fd virus phase. Since channel height is 200 μm and membrane thickness is 60 μm, complete buffer exchanges should occur within few minutes.

As mentioned previously, we observed immediate domain deformation upon increasing salt concentration (Fig. ESI2c,d). For the nematic, present as a single phase in the 0-100 mM NaCl range, tilting the device in respect to the light path showed that dark surfaces were actually nematic domains with an optical axis parallel to the objective. As the nematic phase is uniaxial, a sample with the director normal to the image plane will extinguish light under crossed polarizers. This demonstrates that the rapid decrease in light intensity observed with increasing NaCl concentrations in the nematic phase (Fig. 2a-d) is explained by fd virus reorientation. An optical axis perpendicular to the light path (and parallel to the chamber walls) was favored in low salt concentrations (Fig. 2h) while the optic axis is perpendicular to the sample walls at
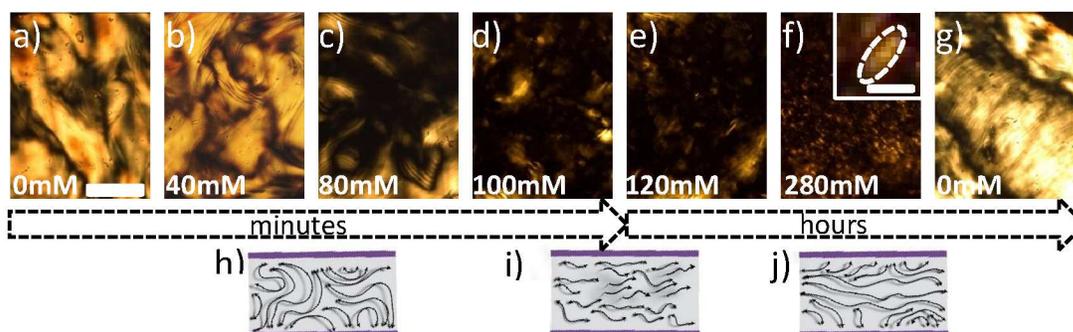
Fig. 2 Cross polarized images (a-j) show the evolution of fd virus system under changing NaCl concentrations. Schematic sketches (h-j) illustrate the reorientation of the optical axis during the experiment, with two typical transition time scales (minutes and hours). For each stepwise change in NaCl concentration, the system was equilibrated before switching salt concentration. A nematic tactoid is circled by a dashed line in the inset. Scale bar 200 μm. Inset scale bar 25 μm. For further information see ESI text.

high concentrations.

Nematic alignment also depended on sample history, as the longest domains were obtained by exchanging from the highest 280 mM NaCl salt concentration directly to 0 mM NaCl. The 280 mM salt isotropic-nematic solution was homogeneously dotted with tactoids (Fig. 2f), and upon the direct exchange to 0 NaCl transformed over hours into large nematic domains of two major groups. Nematic domains near the channel walls had their optical axis vertical to the channel side faces, while nematic domains parallel to the channel's length were formed at the center of the channel (Fig. 2g,j). The parallel domains were over 1 mm long and comparable to channel length (5 mm).

Because all observed phase transitions were reversible, a given fd virus concentration could be loaded once into the chip and then be sequentially probed with multiple salt conditions. In our case, a typical experiment lasted for 3 days, in which about 8 different salt concentrations were tested, for multiple times, against the same virus sample. This strategy allows for the complete phase diagram to be obtained quickly, while also being able to characterize phase transition dynamics, or hysteresis. Due to its modular design, we could re-use the dialysis devices multiple times. After an experiment, the chip was easily disassembled, washed and reassembled with a fresh membrane. Although we did not observe an agglomeration of either myoglobin or fd virus on the channel surface, modifications can be applied on the PDMS to improve its biocompatibility with other substances.[31]

Conclusions

We developed a microfluidic device for micro-liter sample loading and buffer dialysis, compatible with polarization microscopy. We successfully observed a phase transition controlled by buffer exchange through a dialysis membrane in-

tegrated in the device. The design is relatively easy to implement for a variety of time-resolved experiments and creates new opportunities where sample quantities are limited and multiple environmental conditions (e.g. ionic strength, osmolytes, denaturants, pH, and enzymes) need to be accurately controlled and altered. Our chip is modular, easy to fabricate and to operate and reusable. In addition, we demonstrated the applicability of the device using micro-liter amounts of fd virus as a model system. Our results show time scale separation between fast nematic director reorientation and slow phase separation (nematic-isotropic) involving mass transport. Similar behavior was seen when driving the isotropic-nematic transition using magnetic fields or shear flow[32–34]. The advantage of the membrane microfluidic device is that fd virus phase transition boundary can be sampled multiple times using a single specimen, allowing accurate determination of phase boundaries and phase transition hysteresis.

References

1 M. F. G. Wood, N. Ghosh, S.-H. Li, R. D. Weisel, B. C. Wilson, R.-K. Li and A. Vitkin, *SPIE BiOS: Biomedical Optics*, 2009, p. 717908.

2 P. Whittaker, S.-m. Zheng, M. J. Patterson, R. A. Kloner, K. E. Daly and R. A. Hartman, *Lasers in Surgery and Medicine*, 2000, **27**, 305–318.

3 A. J. Howie, D. B. Brewer, D. Howell and A. P. Jones, *Laboratory investigation; a journal of technical methods and pathology*, 2008, **88**, 232–42.

4 N. Schlesinger, *Minerva medica*, 2007, **98**, 759–67.

5 L. Gianaroli, M. C. Magli, A. P. Ferraretti, A. Crippa, M. Lappi, S. Capitani and B. Baccetti, *Fertility and sterility*, 2010, **93**, 807–13.

6 B. Cense, T. C. Chen and J. F. de Boer, *Bulletin de la Société belge d'ophtalmologie*, 2006, 109–21.

7 J. Y. Nam, S. Sinha Ray and M. Okamoto, *Macromolecules*, 2003, **36**, 7126–7131.

8 K. Purdy, S. Varga, A. Galindo, G. Jackson and S. Fraden, *Physical Review Letters*, 2005, **94**, 057801.

9 R. Beck, J. Deek, J. B. Jones and C. R. Safinya, *Nature materials*, 2010, **9**, 40–6.

10 H. C. Hesse, R. Beck, C. Ding, J. B. Jones, J. Deek, N. C. MacDonald, Y. Li and C. R. Safinya, *Langmuir : the ACS journal of surfaces and colloids*, 2008, **24**, 8397–401.

11 S. M. Douglas, J. J. Chou and W. M. Shih, *Proceedings of the National Academy of Sciences of the United States of America*, 2007, **104**, 6644–8.

12 B. H. Chueh, D. Huh, C. R. Kyrtsos, T. Houssin, N. Futai and S. Takayama, *Analytical Chemistry*, 2007, **79**, 3504–8.

13 J. de Jong, R. G. H. Lammertink and M. Wessling, *Lab on a chip*, 2006, **6**, 1125–39.

14 J. Scrimgeour, J. K. Cho, V. Breedveld and J. Curtis, *Soft Matter*, 2011, **7**, 4762.

15 S. Dochow, C. Krafft, U. Neugebauer, T. Bocklitz, T. Henkel, G. Mayer, J. Albert and J. Popp, *Lab on a Chip*, 2011, **11**, 1484–1490.

16 P. M. Fordyce, D. Gerber, D. Tran, J. Zheng, H. Li, J. L. DeRisi and S. R. Quake, *Nature biotechnology*, 2010, **28**, 970–975.

17 K. R. Strehle, D. Cialla, P. Rösch, T. Henkel, M. Köhler and J. Popp, *Analytical Chemistry*, 2007, **79**, 1542–1547.

18 F. Destremaut, J. B. Salmon, L. Qi and J. P. Chapel, *Lab on a Chip*, 2009, **9**, 3289–3296.

19 L. J. Lucas, J.-H. Han, J. Chesler and J.-Y. Yoon, *Biosensors and Bioelectronics*, 2007, **22**, 2216–2222.

20 B. Kuswandi, J. Huskens and W. Verboom, *Analytica chimica acta*, 2007, **601**, 141–155.

21 B. Weinhausen, O. Saldanha, R. N. Wilke, C. Dammann, M. Priebe, M. Burghammer, M. Sprung and S. Köster, *Physical Review Letters*, 2014, **112**, 088102.

22 F. Xiang, Y. Lin, J. Wen, D. W. Matson and R. D. Smith, *Analytical Chemistry*, 1999, **71**, 1485–1490.

23 J. C. McDonald, D. C. Duffy, J. R. Anderson, D. T. Chiu, H. Wu, O. J. A. Schueller and G. M. Whitesides, *Electrophoresis*, 2000, **21**, 27–40.

24 Z. Dogic, K. R. Purdy, E. Grelet, M. Adams and S. Fraden, *Physical review. E, Statistical, nonlinear, and soft matter physics*, 2004, **69**, 051702.

25 K. Zimmermann, H. Hagedorn, C. C. Heuck, M. Hinrichsen and H. Ludwig, *The Journal of biological chemistry*, 1986, **261**, 1653–5.

26 Due to the small free energy difference between nematic and cholesteric phase in relation to the large energy difference between isotropic and nematic phase, we also refer to the cholesteric phase as nematic in this article.

27 J. Sambrook, E. F. Fritsch and T. Maniatis, *Molecular cloning*, Cold spring harbor laboratory press New York, 1989, vol. 2.

28 F. R. Senti, N. N. Hellman, N. H. Ludwig, G. E. Babcock, R. Tobin, C. A. Glass and B. L. Lamberts, *Journal of Polymer Science*, 1955, **17**, 527–546.

29 S. A. Berkowitz and L. A. Day, *Journal of Molecular Biology*, 1976, **102**, 531–547.

30 R. A. Robinson and R. H. Stokes, *Electrolyte Solutions*, Dover Publications, 2002.

31 J. Zhou, A. V. Ellis and N. H. Voelcker, *Electrophoresis*, 2010, **31**, 2–16.

32 J. Tang and S. Fraden, *Physical Review Letters*, 1993, **71**, 3509–3512.

33 M. P. Lettinga, K. Kang, A. Imhof, D. Derks and J. K. G. Dhont, *Journal of Physics: Condensed Matter*, 2005, **17**, S3609–S3618.

34 T. A. J. Lenstra, Z. Dogic and J. K. G. Dhont, *The Journal of Chemical Physics*, 2001, **114**, 10151.